ARTICLE

Corrugation in Exfoliated Graphene: An Electron Microscopy and Diffraction Study

Andrea Locatelli,[†,△,*] Kevin R. Knox,[‡,§,△] Dean Cvetko,[⊥,‖] Tevfik Onur Menteş,[†] Miguel Angel Niño,[†] Shancai Wang,[¶] Mehmet B. Yilmaz,[§,°] Philip Kim,[‡] Richard M. Osgood, Jr.[§,*] , and Alberto Morgante[⊥,#,*]

[†]Elettra, Sincrotrone Trieste S.C.p.A., 34149 Basovizza, Trieste, Italy, [‡]Department of Physics and [§]Department of Applied Physics, Columbia University, New York, New York 10027, [⊥]IOM-CNR Laboratorio TASC, 34149 Basovizza, Trieste, Italy, [‖]Faculty for Mathematics and Physics, University of Ljubljana, Ljubljana, Slovenia, [¶]Department of Physics, Renmin University of China, Beijing, China, [°]Department of Physics, Fatih University, 34500, Buyukcekmece, Istanbul, Turkey, and [#]Department of Physics, Trieste University, Trieste, Italy. [△]Contributed equally to this work.

ABSTRACT Low-energy electron microscopy and microprobe diffraction are used to image and characterize corrugation in SiO_2-supported and suspended exfoliated graphene at nanometer length scales. Diffraction line-shape analysis reveals quantitative differences in surface roughness on length scales below 20 nm which depend on film thickness and interaction with the substrate. Corrugation decreases with increasing film thickness, reflecting the increased stiffness of multilayer films. Specifically, single-layer graphene shows a markedly larger short-range roughness than multilayer graphene. Due to the absence of interactions with the substrate, suspended graphene displays a smoother morphology and texture than supported graphene. A specific feature of suspended single-layer films is the dependence of corrugation on both adsorbate load and temperature, which is manifested by variations in the diffraction line shape. The effects of both intrinsic and extrinsic corrugation factors are discussed.

KEYWORDS: graphene · exfoliated graphene · corrugation · roughness · morphology · μ-LEED · LEEM

Graphene, a single monolayer of carbon atoms arranged in a honeycomb lattice, is attracting exceptional attention in view of potential applications that exploit its unique electronic and transport properties.[1−3] This zero-gap semiconductor is characterized by the linear dispersion of its valence and conduction bands, which meet at inequivalent charge-neutral points in momentum space. Graphene shows an ambipolar electric-field effect and an extremely high mobility of charge carriers, described as relativistic massless fermions, which results in unique transport properties. For instance, single- and double-layer graphene shows anomalous, distinct quantum Hall effects.[4−7] More recently, graphene's unusual chemical properties, which in many cases arise from its reduced dimensionality, have become of interest.[8,9] In particular, the chemical functionalization of graphene opens exciting possibilities for practical engineering of the electronic properties of graphene.[10]

The transport properties of graphene depend strongly on the quality of its crystalline lattice, the presence of defects and dopants, and charge transfer from adsorbed or bound species.[1] Changes in conductance due to molecular adsorption are large enough to permit the detection of individual gas molecules by a graphene sensor.[11] Crystal deformations, due to either intrinsic thermal fluctuations or interactions with the substrate, largely contribute to electron scattering[11] and any attendant decrease in conductivity and carrier mobility.[12−14] In addition, corrugations and defects are expected to affect the chemical properties of graphene. Theoretical studies show that surface defects and bonding irregularities can lower reaction barriers.[15] Extrinsic ripples and curvature can, in fact, produce structure distortions showing domains of lower than hexagonal symmetry.[16] Such domains can exhibit admixture of sp^2 and sp^3 C orbital character and π orbital misalignment, which in carbon nanotubes are known to lead to increased reactivity.[17] Thus, techniques which lead to the control of topographic or morphological defects can play an important role in improving the properties of graphene for applications. For instance, ultrahigh electron mobility was recently achieved in suspended graphene[18] and attributed to the concurrent effects of reduced contamination, the absence of interaction with the substrate, and the decreased surface corrugation.

Considerable experimental and theoretical effort has recently been dedicated to issues related to the morphology of

*Address correspondence to andrea.locatelli@elettra.trieste.it, osgood@columbia.edu, morgante@tasc.infm.it.

Received for review May 20, 2010 and accepted July 20, 2010.

Published online August 3, 2010.
10.1021/nn101116n

© 2010 American Chemical Society

single-layer graphene, addressing in particular the origin of any intrinsic corrugation and its relationship to crystal stability. In one of the earliest of such experiments, transmission electron microscopy revealed that both single- and double-layer suspended graphene display perfect crystalline structure in the short-range but are intrinsically corrugated in the long-range, with deformations in the out-of-plane direction extending to a distance of 1 nm and a surface normal variation of 5°.[19] A recent experimental investigation has shown that long-wavelength ripples in graphene can be controlled by inducing mechanical or thermal strain.[20] However, it is believed that at finite temperature, even in the absence of applied strain, ripples at small wavelengths are present in graphene sheets. In fact, buckling in the direction normal to the lattice plane has been invoked to explain the stability of 2D crystals, as it serves to efficiently suppress long-wavelength phonons,[21−23] which would otherwise cause lattice melting at any finite temperature, as demonstrated by the pioneering work of Peierls,[24] Landau,[25] and later by Mermin.[26] Recent theoretical studies confirm that the intrinsic corrugation in suspended graphene originates from thermal fluctuations and has a well-defined dependence on temperature.[27,28] At sufficiently small length scales, such corrugation is well described by the theory of flexible membranes in the harmonic approximation. At a critical wavelength, estimated to be 20 nm, anharmonic corrections, which couple the bending and stretching modes, become dominant and prevent the membrane from crumpling.[27]

By contrast, corrugations measured in supported graphene are expected to be extrinsic in origin, arising from the interaction of graphene with the substrate. In particular, scanning probe experiments have shown corrugation wavelengths for supported graphene that are in the range of 10−30 nm.[16,29−31] Analyses of the height−height correlation functions in such measurements indicate that graphene has a lower roughness than the SiO_2 support;[16] this arises because the energetic cost of elastic lattice deformation prevents the graphene film from conforming exactly to the substrate topography. In one study of supported graphene using STM, corrugation was reported with a preferential wavelength of 15 nm and attributed to an intrinsic effect[31] since it was not observed on the supporting substrate.

Despite these important advances, further insight into the corrugation of suspended graphene requires measurements at both microscopic and mesoscopic length scales, that is, at length scales from interatomic distances to several hundred nanometers; this large range of length scales has not been examined extensively in previous suspended graphene experiments. STM measurements have provided valuable insights on supported graphene from the microscopic scale up to ~100 nm. However, since STM probing is accompanied by atomic forces due to tip−sample interaction, this technique cannot be easily extended to suspended graphene. Thus, a noninvasive approach is required.

In this paper, we describe such an investigation of the corrugation in both freely suspended and SiO_2-supported exfoliated graphene layers. Our approach takes full advantage of the multiple techniques offered by a low-energy electron microscope (LEEM)[32,33] to obtain a full characterization of the corrugation features in graphene. LEEM allows direct, real-space imaging of the sample morphology over large surface areas (up to several tens of micrometer), with lateral resolution of 10 nm and high structure sensitivity. In addition, this technique enables microprobe low-energy electron diffraction (μ-LEED) measurements that are restricted to a surface area of only a few square micrometers, thus providing access to the reciprocal space. Most importantly μ-LEED is sensitive to crystal deformations on length scales from ~20 nm down to interatomic distances, thus complementing the real-space images by providing additional information about corrugation at very short length scales. By combining these two electron microprobes, we are able to access both the microscopic and mesoscopic regimes and thus the crossover length scale of both intrinsic and extrinsic corrugation.

RESULTS AND DISCUSSION

Imaging of Graphene Film Thickness. An important aspect of our experiments is the ability to measure, *in situ*, the thickness of each graphene sample. Specifically, LEEM can be used to determine precisely the number of layers in thin films by analyzing the modulation in the electron reflectivity between consecutive Bragg peaks at very low electron energy. Such intensity modulation, generally referred to as quantum-size contrast,[34,35] arises due to the quantized energy levels in the film and the formation of quantum-well resonances (QWRs). In the so-called phase accumulation model,[36] QWRs are described by the Bohr−Sommerfeld quantization rule, which sets the condition for a resonance by the existence of constructive interference between electron waves scattered at the film interface and at the surface:

$$2k(E)mt + \Phi_{surf}(E) + \Phi_{if}(E) = 2\pi n \qquad (1)$$

Here, the scalar $k(E)$ is the perpendicular wave vector of an electron in the film, E its energy (relative to the Fermi level), t is the interlayer distance, m is the film thickness (in monolayers), $\Phi_{surf}(E)$ and $\Phi_{if}(E)$ are the energy-dependent phase shifts for reflection of electrons at the surface and at the interface, respectively, and n is an integer. In the case of suspended graphene, $\Phi_{if}(E) = \Phi_{surf}(E)$, the phase shift for reflection at the vacuum interface. The same condition can be assumed to hold in the case of SiO_2-supported graphene, as the graphene film is known to be (partially) suspended on the substrate.[31]

The one-dimensional phase condition described by eq 1 is analogous to that for a resonance in a Fabry–Perot cavity and explains why the LEEM microscope can be effectively used as an electron interferometer for probing the thickness of ultrathin films.[37] Equation 1 can be inverted to determine the existence condition for QWRs.[35,38] In this way, one obtains a formula for the film thickness m, at which QWRs occur as a function of the allowed wave vectors $k(E)$, and the quantum number, ν:

$$m(E, \nu) = \frac{[\Phi_{surf}(E) + \Phi_{if}(E)]/2\pi + \nu}{1 - k(E)t/\pi} \qquad (2)$$

QWRs (and thus maxima in electron reflectivity) are found for $\nu = m - n$, with $1 \leq \nu < m$. Minima in reflectivity are found for $\nu = m - n - 1/2$. It has been shown that $m - 1$ quantum interference peaks, and thus $m - 1$ maxima and m minima in the electron reflectivity, are produced by a film thickness of m layers.[34,38]

Figure 1 (top panel) shows a LEEM image of an area composed of graphene layers of different thicknesses on a SiO_2 substrate, each with a different gray scale intensity. Characteristic LEEM *IV* spectra (obtained in bright-field mode, *i.e.*, using the specular beam) from similar regions with graphene sheets ranging in thickness from 1 to 6 ML are shown in the middle panel of the figure. Solid and open circles in the bottom of Figure 1 indicate the electron energies at which maxima (minima) in electron reflectivity are observed, respectively. As can be seen, the predictions of the phase accumulation model obtained using eq 2, represented by continuous (dashed) curves in the figure, match the experimental data closely. Details of the calculations are given in the Methods section.

The intensity modulations in the *IV* spectra of exfoliated multilayer graphene samples closely resemble the previously reported spectra of epitaxial graphene on SiC.[39,40] The single-layer LEEM *IV* spectrum of SiO_2-supported graphene (dashed curve in Figure 1, middle) is instead completely featureless. The identification of this featureless spectrum with single-layer graphene is confirmed by LEED measurements, which show a clear 6-fold symmetry, in contrast to the 3-fold symmetry observed for multilayer samples. As expected, no Bragg peaks were observed in the LEED *IV* spectrum of single-layer graphene. In fact, no such peaks can be seen for suspended or SiO_2-supported single-layer graphene, as the Bragg condition originates from constructive interference between waves scattered at different crystal planes.

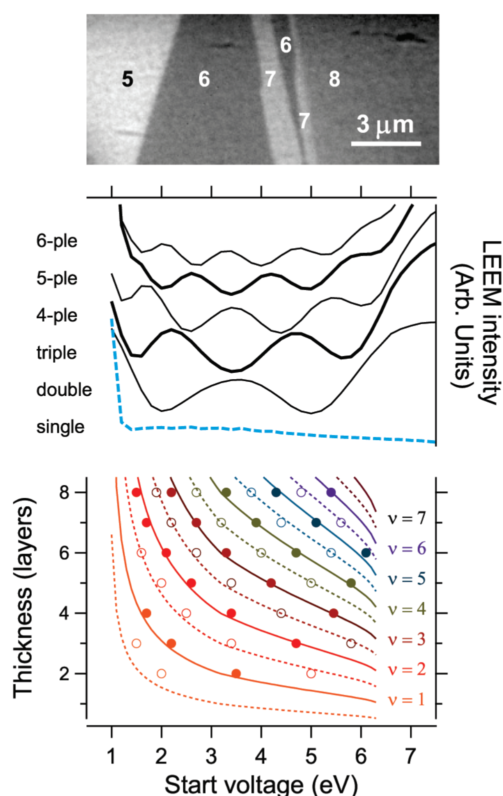

Figure 1. (Top) LEEM image of a multi-thickness graphene sheet supported on SiO_2: the local thickness is indicated by the labels; (middle) LEEM *IV* spectra of supported graphene films of differing thicknesses. The spectra demonstrate large variations in the electron reflectivity as a function of the electron kinetic energy (start voltage). The intensity modulations observed in multilayer samples (continuous lines) are induced by electron confinement. The curves have been offset for clarity. (Bottom) Solid (open) circles identify the electron kinetic energies and film thicknesses at which maxima (minima) in electron reflectivity are observed. The continuous (dashed) lines represent the predictions for such maxima (minima), obtained using eq 2 for different quantum numbers ν, with the film thickness treated as a continuous variable.

LEEM Imaging of Graphene Corrugation. Due to its high lateral resolution and thickness sensitivity, LEEM provides access to the local morphology of suspended and supported graphene samples. Figure 2 shows LEEM images of a large multi-thickness graphene flake on the SiO_2 substrate, into which micrometer-sized cylindrical cavities have been etched, as described in the Methods section. The disks correspond to the suspended portions of the film. The variation in the local thickness of the film (indicated by labels in Figure 2A) becomes evident at an electron kinetic energy of 4.2 eV, due to the quantum-size contrast. In all samples under study and for all thicknesses examined, the suspended portions of our samples appeared brighter in LEEM than those supported on SiO_2. This is consistent with the reduced intensity and broader width of the zero-order diffraction *IV* curves recorded on all SiO_2-supported samples (see Figure 2). This type of contrast arises due to surface corrugation because the finite angular acceptance of the microscope rejects e-beam reflections from surface planes tilted beyond the cutoff angle as determined by a contrast aperture.[41] Thus, a surface that scatters the e-beam over a wide range of off-normal angles will appear darker than a flat one, aligned normal to the beam. We note that this effect occurs even if the wavelength of the corrugation is below the lateral resolution of the microscope.

LEEM images at higher magnification show clearly the origin of the contrast difference observed between suspended and supported regions. High lateral resolution images of single, double, and trilayer graphene are shown in Figure 3A–C. The higher reflectivity of the single-layer suspended disk (A) is due to the presence of large flat regions normal to the e-beam (appearing bright in the figure), which in some cases extend up to lengths of about 50 nm. These bright areas are fewer and smaller on the supported part of the film but become larger on thicker samples. We observe that the patterns in Figure 3 change when tilting the e-beam illumination, which causes different surface planes to become visible. This behavior confirms that the contrast observed in LEEM arises from variations in the local surface normal of a static smooth surface. It can be argued that the more pronounced corrugation observed in supported regions might be induced by the interaction with the substrate[16,29−31] and therefore is extrinsic in origin. Adsorbates are another possible source of corrugation. It is, in fact, known that even small quantities of impurities can determine crystal deformation, as has been pointed out in a recent STEM study.[42]

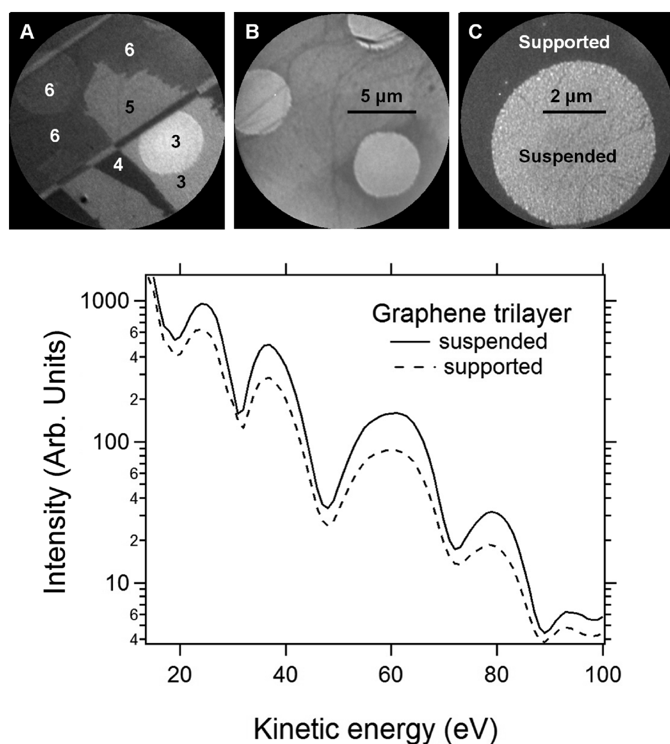

Figure 2. (A) LEEM image at 4.2 eV of suspended disks and SiO_2-supported graphene (disk diameter is 5 μm). The local thickness, in units of graphitic layers (indicated by labels), was determined by measuring the electron reflectivity curves in the energy interval of 1 to 8 eV; (B) LEEM image of the same region at electron kinetic energy of 38 eV; (C) LEEM image of the suspended portion of the single-layer region at electron kinetic energy of 10 eV. (Bottom) Zero-order diffraction LEED *IV* curves of SiO_2-supported and suspended trilayer graphene.

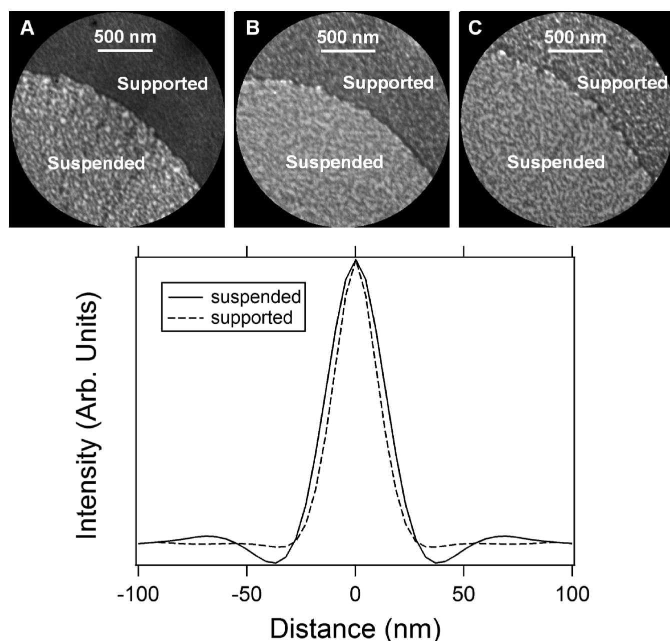

Figure 3. (A–C) LEEM images at 10 eV illustrating the morphology of suspended and SiO_2-supported graphene: (A) single layer, (B) bilayer, and (C) trilayer suspended graphene disks and surrounding supported areas. (Bottom) Intensity autocorrelation function curves of the SiO_2-supported (dashed line) and suspended regions shown in (A).

Although LEEM cannot provide absolute height information, the LEEM images in Figure 3 can be used to estimate the horizontal correlation length. The bright regions correspond to clean *flat* areas, where local height variations are small and correlated (we note that different bright regions may have different heights). Thus, the horizontal correlation length ξ (*i.e.*, the distance beyond which height fluctuations are no longer correlated) corresponds to the average size and distribution of these bright regions. We have computed ξ by measuring the full width at half-maximum of the autocorrelation function central peak from intensity profiles taken across the LEEM images (see the lower part of Figure 3). In this way, we find values of 24 ± 0.3 and 30 ± 0.3 nm for single-layer supported and suspended graphene, respectively, which increase to ~36 nm for both supported and suspended bilayer graphene. Our value of 24 nm for supported single-layer graphene compares favorably to previously reported correlation lengths measured by STM on SiO_2-supported graphene, which vary in the range of 10 to about 30 nm.[16,29,31] The weak oscillations observed in the autocorrelation function of single-layer suspended regions (see Figure 3) reveal a preferential ripple wavelength of several tens of nanometers (~60 nm), which points to the *mounded* nature of the suspended graphene surface.

Finally, we note that the high lateral resolution LEEM images in Figure 3A–C clearly show that the disk edges appear rough. This roughness, which is due to the imperfect edge definition of the etched well, indicates that graphene has the flexibility to conform to edge surface features at the 10 nm scale. In addition, a close examination of the images also reveals the presence of darker lines (resembling veins) extending across the graphene throughout the supported and suspended re-

gions. As can be seen by comparing Figure 2A,B, these are not steps separating regions of different thickness. The origin of these features could be short wavelength wrinkles in the graphene membrane, in accord with similar observations reported in a recent STEM study.[42]

LEED Measurements of Surface Corrugation. Due to the intrinsic sensitivity of the line shape of diffracted electron beams to local height variations, microprobe low-energy electron diffraction (μ-LEED) was used to probe the roughness of SiO_2-supported and suspended regions of uniform thickness. In particular, μ-LEED measurements allowed us to access lattice distortions at length scales below the horizontal correlation length (few tens of nanometers in single- and double-layer graphene), thus complementing the LEEM data presented in the previous section.

The most prominent feature that was observed in all graphene samples was the broadening of the diffraction profile with increasing perpendicular electron momentum transfer. Figure 4 shows profiles of the central diffraction beam of single-layer suspended graphene at multiple kinetic energies, together with best fits obtained using a multidimensional Lorentzian. This line shape provides an excellent approximation to the expected diffraction line shape for rough surfaces (see the Supporting Information provided). The fit function was convolved with a Gaussian in order to take into account the response function of the instrument, which has a transfer width of 10 nm. This width is constant within the energy range of pertinence to this study.

Figure 5 shows the variation of the half width at half-maximum (hwhm) of the (00) diffraction beam as a function of increasing perpendicular momentum transfer of the probe electrons, $k_\perp = (\mathbf{k}_{in} - \mathbf{k}_{out})\hat{n} \cong 2|\mathbf{k}_{in}|$, for SiO_2-supported and suspended graphene (left and right panels in the figure, respectively). Each data point in the figure was obtained by fitting the (00) diffraction beam with a multidimensional Lorentzian line profile, as shown in Figure 4. As can be seen, film thickness and the presence of a supporting substrate have a significant influence on the evolution of peak broadening. We observe that peak broadening is always less pronounced in suspended than in supported samples. For example, suspended bilayer graphene films show such narrow diffraction peaks that their widths are comparable to those of thick supported graphite films.

The broadening of the central diffraction peak with increasing $k_\perp$ is not observed on thick graphite films on SiO_2 (which are expected to be atomically flat) that have undergone the same preparation and cleaning procedure as that used for graphene (see the curve labeled TG in Figure 5). For all graphite flakes, the hwhm was less than 0.05 $Å^{-1}$, and nearly independent of $k_\perp$. This value is considerably smaller than that measured on SiO_2-supported and suspended single-layer graphene ($\geq$0.45 $Å^{-1}$ at $k_\perp$ =8 $Å^{-1}$).

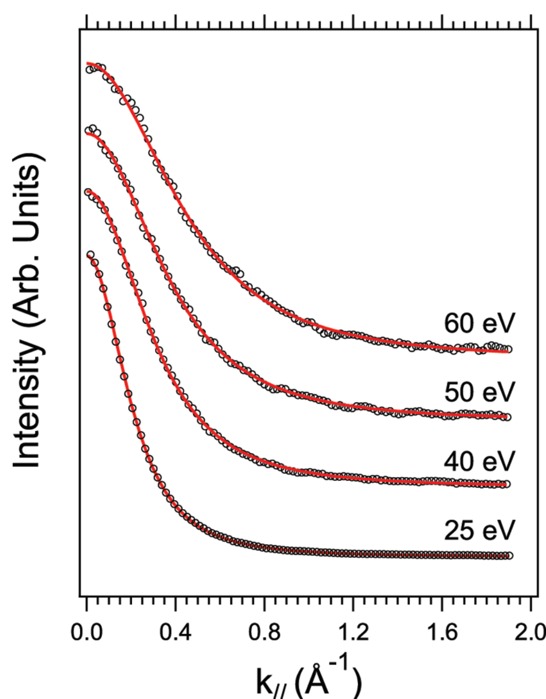

Figure 4. Profile across the (00) diffraction beam of single-layer suspended graphene at multiple electron energies. Multidimensional Lorentzian fits are shown as solid lines. See text for details. The curves have been offset for clarity.

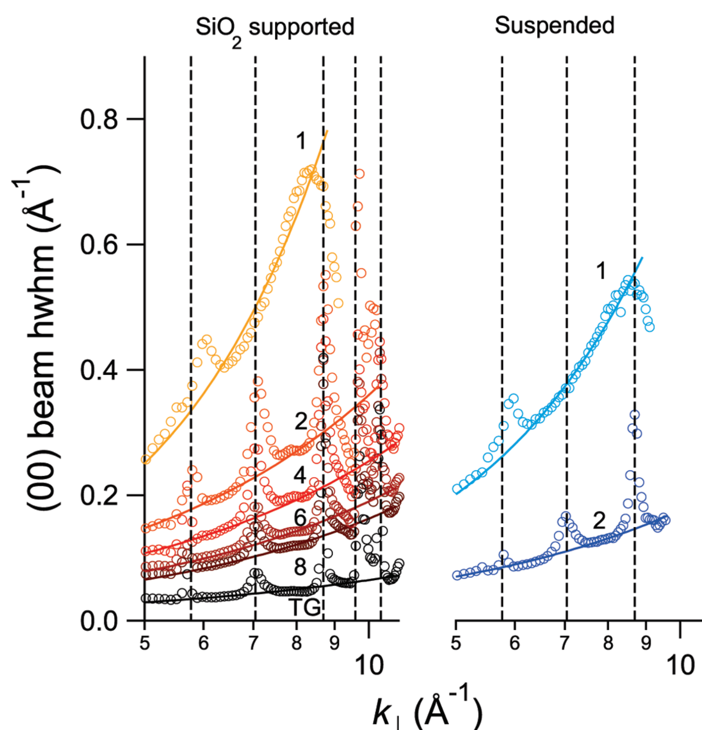

Figure 5. Variation of the (00) diffraction beam hwhm (circles) for different graphene films as a function of the electron momentum transfer $k_\perp$, measured at room temperature. The dashed vertical lines indicate resonances corresponding to out-of-phase diffraction conditions in multilayers. The continuous lines represent best fits using eq 3. The hwhm curves for SiO_2-supported and suspended graphene are shown in the left and right panels, respectively. The film thickness is indicated by the numeric labels; TG refers to thick graphite film on SiO_2.

All curves in Figure 5 show the presence of several sharp peaks in the width of the central diffraction beam (indicated by the dashed vertical lines in the figure). In single-layer graphene, such peaks are observed when higher-order diffraction spots enter the Ewald sphere. For instance, at $k_\perp = 5.8$ Å^{-1} and $k_\perp \sim 9.7$ Å^{-1}, the peak width of the zeroth order diffraction beam reaches distinct maxima, which correspond to a sharp decrease in the diffraction intensity due to the appearance of the first- and second-order diffraction spots, respectively. In multilayer films, additional maxima in peak width can be observed at electron wavelengths that correspond to out-of-phase diffraction conditions, that is, to maximum destructive interference between waves that are backscattered at the different layers. We observe that, under these conditions, the diffraction line shape cannot be described in a simple way as arising from local height variations of the graphene surface because other contributions to broadening may come into play (*e.g.*, inelastic scattering, diffuse elastic scattering due to correlation between adsorbates or defects; we can exclude broadening due to the amorphous SiO_2 substrate, as no evidence of zero-order diffraction can be observed on it). Therefore, data points corresponding to these values of $k_\perp$ were not considered in the analysis that follows.

Quantitative Analysis of the Short-Range Roughness in Graphene. The analysis of the angular intensity distribution of diffraction data is a powerful investigative tool for characterizing surface disorder and roughness on a vast class of systems, including random, self-affine, and mounded surfaces.[43,44] Relevant examples of application can be found in epitaxial growth processes.[45−48] As will be shown below, LEED line-shape analysis allowed us to estimate an important parameter that is commonly used to quantify surface roughness, the *roughness exponent* α. This parameter describes the short-range behavior of the height−height correlation function, which, below horizontal correlation length, scales as a power law with exponent 2α. In fact, α measures surface roughness. It ranges from 0 to 1: small (large) values indicate jagged (smooth) morphology on short length scales.

The data set presented in Figure 5 allows us to determine accurately the dependence of broadening on momentum transfer, demonstrating that the zero-order diffraction width increases according to a power law (continuous lines). Deviations from linearity are small and become important only in the case of single-layer graphene. This behavior can be understood invoking the model developed by Yang, Wang, and Lu,[43,44,49] which describes the general principles of diffraction from rough surfaces (a summary of the model can be found in the Supporting Information provided). This kinematic model predicts that the diffraction line shape, which is connected to the height−height correlation function of the rippled surface by a Fourier transform, can be expressed as a function of the parameters describing roughness on self-affine surfaces. For sufficiently large perpendicular momentum transfer $k_\perp$, the diffraction profile does not show a δ function character but becomes purely diffusive (*i.e.*, broadened). This occurs when $\Omega \equiv (wk_\perp)^2 \gg 1$, where w, referred to as interface width, is the standard deviation of the surface height.[50] In this case, the hwhm of the zero-order diffraction scales according to a power law of the electron momentum transfer $k_\perp$:[43]

$$\mathrm{hwhm}(00) = Z_g \eta^{-1} k_\perp^{1/\alpha} \quad (3)$$

Z_g defines the half width of the scaling function that determines the actual shape of the peak profile. The parameter η (roughness length) also describes roughness in the short range and is defined as: $\eta = \xi w^{-1/\alpha}$. From this definition, it follows that η is proportional to the average width of correlated areas (*i.e.*, the flat regions in the continuously bent graphene film). Note that η is not dimensionless, but $\eta = [L]^{(\alpha-1)/\alpha}$ (where L is a length).

Rigorously, eq 3 is only valid for self-affine surfaces.[43] It is unclear whether graphene can be considered purely self-affine. In the case of thin supported films, self-affinity might be inherited from the SiO_2 substrate, to which the graphene partially conforms. Suspended as well as thicker supported films show different characteristics. The oscillatory behavior in the autocorrelation function observed in single-layer suspended graphene (see for example Figure 3) suggests that the large wavelength ripples show a preferential periodicity, so that the surface can be more appropriately considered as *mounded*. In this case, the hwhm is expected to depend on both the correlation length and ripple wavelength.[48] However, we observe that, for sufficiently large values of the momentum transfer, diffraction theory predicts that peak broadening results from corrugations at length scales much smaller than the correlation length.[44] Thus, the effect of the surface curvature at large wavelengths can be neglected and eq 3 can be safely assumed to hold validity.

Experimentally, the roughness exponent α was obtained by fitting the data in Figure 5 using eq 3. The data points corresponding to the out-of-phase diffraction condition were not included in the fit for a two-fold reason. (i) Other broadening contributions may become important, as anticipated; (ii) one of the hypotheses that form the basis of Yang's model does not hold, and the model cannot be applied. Z_g was calculated numerically after finding α (see the Supporting Information), which allowed us to determine the short-range parameter η. The values of α and η for suspended and supported graphene are shown in Table 1 as a function of film thickness. As can be seen, two distinct regimes can be identified corresponding to single- and multilayer graphene. For single-layer graphene, we measure values of α close to 0.5. This value is consistent with the roughness exponent of the height−height correlation

TABLE 1. Roughness Exponent α and Roughness Parameter η as a Function of Film Thickness for Supported and Suspended Graphene at Room Temperature (TG is for Thick Graphite Films Supported on SiO_2; η is in Units of $[Å]^{(\alpha-1)/\alpha}$)

	SiO_2-supported		suspended	
thickness (layers)	α	η	α	η
1	0.49 ± 0.04	77 ± 20	0.54 ± 0.02	84 ± 11
2	0.80 ± 0.04	64 ± 6	0.80 ± 0.05	144 ± 25
3	0.80 ± 0.06	81 ± 14	0.82 ± 0.06	131 ± 24
4	0.77 ± 0.07	104 ± 28		
6	0.80 ± 0.05	133 ± 25		
8	0.80 ± 0.05	157 ± 25		
TG	0.87 ± 0.07	327 ± 70		

function reported in two recent scanning probe studies.[16,31] The rougher short-range morphology of single-layer supported graphene results from the interaction with the SiO_2 substrate, to which the graphene partially conforms.[31] Conversely, in both suspended and SiO_2-supported multilayers, α saturates to ~0.8. Note that a similar value of α is observed even at bilayer thickness, which suggests that the increased stiffness of the bilayer is already sufficient to warrant a smooth short-range morphology. The smoother texture of supported multilayers is confirmed by the monotonic increase of η with film thickness.[51] This suggests that the films become progressively flatter with increasing thickness. Large values of η are observed in the case of suspended graphene even at bilayer thickness, suggesting the presence of very large *flat* regions (namely, areas over which the height−height correlation function is constant). Finally, we observe that the rough short-range morphology of SiO_2-supported single-layer graphene reported in this study is consistent with the broadening of the momentum distribution curves previously observed in microprobe angle-resolved photoelectron spectroscopy experiments on the same system.[52]

Effect of Adsorbates and Temperature Dependence. We now discuss the effect of electron and photon irradiation on the LEED peak width in single and bilayer suspended graphene. As reported in the methods section, our samples were treated using electron stimulated desorption (ESD). Figure 6, left panel, shows the hwhm vs $k_\perp$ of single and bilayer films, for different exposures to electron and photon beams. Open circles (curves labeled A) indicate hwhm data that were acquired shortly after the standard preparation procedure used in this study, which corresponds to an irradiation time of 30 min with 60 eV electrons (see the methods section). The other curves (labeled B, open triangles) were measured after much longer irradiations with electrons (about 3 h and 30 min, at energy >10 eV) and photons (~ 50 eV, for about 1 h). As can be seen, only suspended single layer graphene displays a notable narrowing of the peak width after prolonged irradiation.

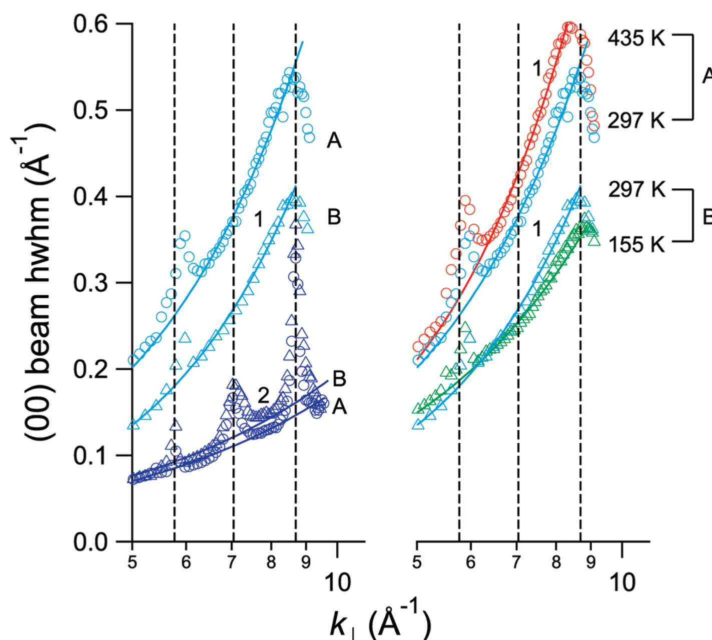

Figure 6. Left: variation of the (00) diffraction beam hwhm for single- (1) and double-layer (2) suspended graphene at room temperature, as a function of the electron momentum transfer $k_\perp$. The curves labeled A (open circles) were measured after irradiating the film for 30 min with 60 eV electrons. Curves B (open triangles) were measured after a longer irradiation (see text). Right: hwhm curves of single-layer suspended graphene at different temperatures, for different exposures to e-beam (A and B). Sample temperature is indicated by the labels.

Conversely, the hwhm curves of suspended bilayer disks do not differ appreciably before and after long irradiation. The LEED peak narrowing observed in single layer graphene results from an increase in value of the parameter η, rather than that of α (see Table 2). Thus, we can relate the narrowing of the zero-order diffraction to the improved sample cleanliness that was achieved by ESD. We argue that the roughness may vary significantly as a result of small variations in adsorbate concentration, due to the reduced stiffness of single-layer films. This suggests that the corrugation in single-layer exfoliated graphene can be affected by adsorbates and thus is, at least in part, extrinsic in origin.

In order to gain a more detailed understanding of the corrugation in graphene, we investigated the effect of temperature change on the LEED peak broadening in suspended single-layer and bilayer films. Contrary to bilayer graphene, single-layer graphene displays temperature-induced changes in the shape of the zero-order diffraction peak. The effect of temperature on line broadening of single-layer graphene is shown in the right panel of Figure 6, for short (A) and long (B) e-beam irradiation times. The curves at high and low temperatures were acquired after those at room temperature. As can be seen in both cases, a change in sample temperature leads to a noticeable change in the slope of the hwhm *versus* $k_\perp$. Peak-profile analysis shows that, independent of electron and photon irradiation time, the roughness parameter α in-

TABLE 2. Roughness Exponent α and Roughness Parameter η as a Function of Film Thickness for Suspended Graphene at Different Temperatures and for Different Irradiations Times: (A) Irradiation of 30 min with 60 eV Electrons; (B) Irradiations with Electrons (about 210 min, at Energy >10 eV) and Photons (~50 eV, for about 1 h); η is in Units of $[\text{Å}]^{(\alpha-1)/\alpha}$

		short irradiation (A)		long irradiation (B)	
thickness (layers)	temperature (K)	α	η	α	η
1	435	0.49 ± 0.02	94 ± 11		
1	297	0.54 ± 0.02	84 ± 11	0.50 ± 0.02	143 ± 23
1	155			0.64 ± 0.03	91 ± 11
2	435	0.73 ± 0.08	153 ± 50		
2	297	0.80 ± 0.05	144 ± 25	0.74 ± 0.07	150 ± 50
2	155			0.78 ± 0.06	96 ± 19

creases with decreasing temperature (see Table 2) and reaches a maximum value of 0.64 at 155 K. Thus, temperature-induced changes in peak broadening can be clearly resolved from those induced by adsorbates, which affect η. The observed variation of α suggests that the film roughness decreases at wavelengths well below horizontal correlation length and coherence of the probe electron beam (~20 nm in both cases). In this instance, LEED peak narrowing is due to an increase of coherent scattering at short wavelengths, which we attribute to a reduced deformation of the lattice at low temperature.

It is important to note that the Debye–Waller effect is not expected to produce a broadening of the diffraction peaks. Increasing vibrational amplitudes, in fact, leave the average lattice constants unchanged and therefore simply result in a decrease of the diffraction intensity.[53] Our results are in agreement with the theory of Fasolino, which predicts that phonon-induced corrugations in graphene should occur on length scales below 20 nm. Such corrugations, which may be related to the different bond lengths arising from the multiplicity of the carbon bond, display a well-defined dependence on temperature.[27] In fact, in the harmonic approximation, the rms height variation across a flexible membrane scales with temperature as $(T/\kappa(T))^{1/2}$, where $\kappa(T)$ is the bending rigidity. A detailed comparison with theoretical predictions for the above functional dependence is impossible in our case because of the interplay between intrinsic and extrinsic factors. We underline that the effect of temperature is smaller than that of adsorbates. This warrants the need for additional, detailed investigations in order to discriminate the different effects of temperature, adsorbate loading, and substrate configuration.

CONCLUSIONS

LEEM and μ-LEED measurements were used to characterize the surface morphology, local thickness, and crystal structure of suspended and SiO_2-supported graphene layers. Our results show clearly that the corrugation observed on supported graphene samples is quantitatively different than that observed on suspended samples. While the former is largely determined by the morphology of the substrate, the latter is influenced by intrinsic and extrinsic factors. Supported graphene samples display a rough morphology at short wavelengths, up to a thickness of several layers. This corrugation decreases with increasing film thickness, as the stiffer multilayer film becomes effectively suspended on the hills of the SiO_2 substrate.

Suspended samples appear significantly smoother in the short range than those supported on SiO_2. For instance, bilayer suspended graphene shows very narrow diffraction peaks, comparable to those measured on thick supported graphite films. The smooth short-range texture of suspended bilayer is confirmed by the high value of the roughness exponent (~0.8). Microprobe diffraction measurements demonstrate, however, that suspended single-layer graphene films are still corrugated. The roughness exponent, ~0.55 at room temperature, is lower than that measured on multilayers. We note that the reduced corrugation of suspended graphene reported here correlates well with the significantly improved transport properties of suspended graphene devices.[18]

Most relevantly, our experiments provide evidence that the corrugation in single-layer suspended graphene is sensitive to adsorbate load and temperature variations. This behavior, which is characteristic of single-layer graphene, is determined by the very high flexibility of the crystal at this thickness. The weak temperature dependence of the diffraction line shape observed in single-layer disks points to a line broadening mechanism that is only partially phonon-induced, and thus intrinsic in nature, which supports the picture that thermal fluctuations produce deviations from planarity.[27] However, we underline that the most important contributions to corrugation in single-layer exfoliated graphene are extrinsic. Our results, in fact, suggest that interactions with physisorbed or chemisorbed species can cause significant changes in the surface morphology. We envisage that the ability to modify such corrugation, by means of temperature, boundary conditions, deposition or removal of host adatoms and molecules *etc.*, will be crucial in assuming further control of the transport properties of graphene, with important implications to the their future exploitation in practical devices.

METHODS

Electron Microscopy Measurements. LEEM is a structure-sensitive technique that uses elastically backscattered electrons to image a crystalline surface. All measurements described here were made using the spectroscopic photoemission and low-energy electron microscope (SPELEEM, Elmitec, GmbH) in operation at the Elettra Synchrotron Laboratory. The instrument combines LEEM imaging with low-energy electron diffraction (μ-LEED) and chemically sensitive energy filtered photoemission electron microscopy (XPEEM). The microscope achieves its highest lateral resolution (10 nm) when operated in LEEM mode[54] and allows sample cooling to a minimum temperature of 155 K. The transfer width of the microscope is equal to 10 nm. This value was obtained by measuring the width of the LEED primary beam on a step-free region of a clean W(110) crystal.[55] The instrumental response function of the microscope has been found to be predominantly Gaussian.

All microprobe diffraction measurements were restricted to circular regions 2 μm in diameter on defect-free, micrometer-sized, well-defined single thickness graphene samples. This approach allowed us to illuminate only the central part of the suspended graphene disks (diameter of 5 μm) to avoid any edge effects induced by the boundary. On supported samples, the current density was kept to a minimum (less than 1 pA/μm^2) in order to prevent charging of the oxide substrate. For LEEM imaging, larger illumination apertures were used, allowing us to image both the supported and suspended portions of the graphene flakes while avoiding illuminating the SiO_2 region that surrounds them. Due to low-electron energy range used (≤80 eV), LEEM and LEED are not expected to produce appreciable surface damage. Further, due to the noninvasive interaction, they are unlikely to perturb the morphology of suspended graphene sheets.

Phase Accumulation Model. Predictions for the energy of reflectivity maxima and minima were obtained with the phase accumulation model,[35,38] by imposing the condition for the film thickness m at which quantum-well resonances occur as a function of the allowed wave vectors k and the quantum number ν (see eq 2). In our calculation, the phase shifts upon electron reflection at the surface, which represents the leakage of the standing wave function beyond the boundary, were assumed to be equal to 0. This approximation, which is essentially phenomenological, has been widely used in previous studies.[35,38] The phase shift at the other surface plane was treated identically, as both terminating planes of the graphene films are, in fact, equal in the case of suspended samples. The same holds in the case of supported samples because the interface is partially suspended and the interaction with the SiO_2 supporting substrate is minimal. We recall here that the LEEM *IV* curves for suspended and supported samples are identical.

The function $k(E)$ was obtained by modeling the conduction band of graphite in the ΓA direction using the simple tight-binding scheme (*i.e.*, $E = \varepsilon - 2t\cos(ka)$), where ε is the energy of the band center, a is the interlayer distance, and t is 1/4 of the bandwidth.[39] The electron energy E is referenced to the Fermi level and is given by $E = (E_{kin} - E_{vac}) + \phi$, where E_{kin} is the kinetic energy (often referred to as *start energy*) of the electrons impinging on the surface, E_{vac} is the vacuum level (obtained as the energy of the transition from LEEM to total reflection, ~0.75 eV in our case), and ϕ is the work function of graphite (*i.e.*, 4.65 eV).[57]

The band parameters (band minimum and maximum) were adjusted to optimize the fit with the experimental data. The curves shown in Figure 1 (bottom-right) reproduce the position of experimental maxima and minima in electron reflectivity with very good accuracy. They were obtained with E_L and E_T equal to 5 and 10.4 eV (relative to the Fermi level). These values compare reasonably well with 4.4 and 10.7 eV reported in a recent *ab initio* study on multilayer graphene.[39]

Sample Preparation. The graphene samples were obtained by micromechanical cleavage technique from Kish graphite crystals (Toshiba Ceramics, Inc.) and placed onto a 300 nm SiO_2/Si substrate. The use of a patterned substrate, in which cylindrical cavities 5 μm in diameter were etched to a depth of 500 nm, enabled large areas of graphene layers to be effectively suspended. Great care was taken to eliminate any source of surface contamination during sample preparation, ensuring that the graphene surface under study was pristine. In particular, we stress that no photolithographic patterning techniques were used on the graphene sheets. To avoid charging the substrate under photon and electron beam irradiation, the graphene flakes were grounded by Au/Cr stripes evaporated through a metal shadow mask. Prior to the experiments with the electron microscope, all samples were inspected with an optical microscope to identify the thinnest flakes.[56]

Sample Cleaning Procedure. Several experiments were carried out to determine the best surface preparation procedure for the graphene. It was found that prolonged UHV annealing at 300 °C resulted in degradation of the graphene LEED pattern, possibly due to the oxidation of the graphene due to the interaction with the underlying SiO_2 substrate.[9] Further, XPEEM measurements showed that heating caused diffusion of Au and Cr across the graphene from the nearby grounding stripes. These two problems prevented us from cleaning samples by annealing. Electron-stimulated desorption of the adspecies was chosen instead for *in situ* surface preparation. In fact, irradiation at room temperature with low-energy electrons (in the range of 25−150 eV) was found to result in a rapid increase in the intensity of the LEED patterns of both graphite and graphene flakes. The samples were locally irradiated until the electron reflectivity of the Bragg reflection at 60 eV reached maximum intensity, typically in ~30 min. As the samples were chosen not to be treated thermally, we cannot exclude the presence of impurities, carbonates in particular, on the films. Comparative LEEM experiments were also carried out on HOPG; these experiments verified that irradiation with 60 eV electrons produced very sharp LEED patterns and led to the development of clean areas as large as 1 μm. The experiments on HOPG also showed that after e-beam irradiation some degree of contamination remained in the form of islands nucleated at steps, step bunches, or other surface defects.

Acknowledgment. K.R.K. and S.W. acknowledge support for materials and sample preparation from the NSF Award Number CHE-0641523 and by NYSTAR; R.M.O., K.R.K., and S.W. acknowledge support from DOE BES (Contract No. DE-FG02-04-ER-46157) for travel and experimental work. The synchrotron portion of the project (A.M., D.C.) at Elettra was supported also through MiUR-PRIN2008-prot.20087NX9Y7_002. A.M. gratefully acknowledges the NSEC at Columbia University and the Italian Academy at Columbia University for the warm hospitality and financial support during his visit. P.K. acknowledges support from AFOSR MURI.

Supporting Information Available: Diffraction from rough graphene surfaces. This material is available free of charge *via* the Internet at http://pubs.acs.org.

REFERENCES AND NOTES

1. Castro Neto, A. H.; Guinea, F.; Peres, N. M. R.; Novoselov, K. S.; Geim, A. K. The Electronic Properties of Graphene. *Rev. Mod. Phys.* **2009**, *81*, 109–163.
2. Geim, A. K.; Novoselov, K. S. The Rise of Graphene. *Nat. Mater.* **2007**, *6*, 183–191.
3. Geim, A. K.; Kim, P. Carbon Wonderland. *Sci. Am.* **2008**, *298*, 90–97.
4. Novoselov, K. S.; Geim, A. K.; Morozov, S. V.; Jiang, D.; Katsnelson, M. I.; Grigorieva, I. V.; Dubonos, S. V.; Firsov, A. A. Two-Dimensional Gas of Massless Dirac Fermions in Graphene. *Nature* **2005**, *438*, 197–200.
5. Novoselov, K. S.; McCann, E.; Morozov, S. V.; Falko, V. I.; Katsnelson, M. I.; Zeitler, U.; Jiang, D.; Schedin, F.; Geim, A. K. Unconventional Quantum Hall Effect and Berry's Phase of 2π in Bilayer Graphene. *Nat. Phys.* **2006**, *2*, 177–180.
6. Zhang, Y.; Tan, Y.-W.; Stormer, H. L.; Kim, P. Experimental Observation of the Quantum Hall Effect and Berry's Phase in Graphene. *Nature* **2005**, *438*, 201–204.
7. Novoselov, K. S.; Jiang, Z.; Zhang, Y.; Morozov, S. V.; Stormer, H. L.; Zeitler, U.; Maan, J. C.; Boebinger, G. S.; Kim,

P.; Geim, A. K. Room-Temperature Quantum Hall Effect in Graphene. *Science* **2007**, *315*, 1379.
8. Ryu, S.; Han, M. Y.; Maultzsch, J.; Heinz, T. F.; Kim, P.; Steigerwald, M. L.; Brus, L. E. Reversible Basal Plane Hydrogenation of Graphene. *Nano Lett.* **2008**, *8*, 4597–4602.
9. Liu, L.; Ryu, S.; Tomasik, M. R.; Stolyarova, E.; Jung, N.; Hybertsen, M. S.; Steigerwald, M. L.; Brus, L. E.; Flynn, G. W. Graphene Oxidation: Thickness-Dependent Etching and Strong Chemical Doping. *Nano Lett.* **2008**, *8*, 1965–1970.
10. Ruoff, R. Calling All Chemists. *Nat. Mater.* **2008**, *3*, 10–11.
11. Schedin, F.; Geim, A. K.; Morozov, S. V.; Hill, E. W.; Blake, P.; Katsnelson, M. I.; Novoselov, K. S. Detection of Individual Gas Molecules Adsorbed on Graphene. *Nat. Mater.* **2007**, *6*, 652–655.
12. Gazit, D. Theory of the Spontaneous Buckling of Doped Graphene. *Phys. Rev. B* **2009**, *79*, 113411.
13. Mariani, E.; von Oppen, F. Flexural Phonons in Free-Standing Graphene. *Phys. Rev. Lett.* **2008**, *100*, 076801.
14. Katsnelson, M. I.; Geim, A. K. Electron Scattering on Microscopic Corrugations in Graphene. *Philos. Trans. R. Soc. London, Ser. A* **2008**, *366*, 195–204.
15. Xu, S. C.; Irle, S.; Musaev, D. G.; Lin, M. C. Quantum Chemical Study of the Dissociative Adsorption of OH and H_2O on Pristine and Defective Graphite (0001) Surfaces: Reaction Mechanisms and Kinetics. *J. Phys. Chem. C* **2007**, *111*, 1355.
16. Ishigami, M.; Chen, J. H.; Cullen, W. G.; Fuhrer, M. S.; Williams, E. D. Atomic Structure of Graphene on SiO_2. *Nano Lett.* **2007**, *7*, 1643–1648.
17. Niyogi, S.; Hamon, M. A.; Hu, H.; Zhao, B.; Bhowmik, P.; Sen, R.; Itkis, M. E.; Haddon, R. C. Chemistry of Single-Walled Carbon Nanotubes. *Acc. Chem. Res.* **2002**, *35*, 1105–1113.
18. Bolotin, K. I.; Sikes, K. J.; Jiang, Z.; Fudenberg, G.; Hone, J.; Kim, P.; Stormer, H. L. Ultrahigh Electron Mobility in Suspended Graphene. *Solid State Commun.* **2008**, *146*, 351–355.
19. Meyer, J. C.; Geim, A. K.; Katsnelson, M. I.; Novoselov, K. S.; Booth, T. J.; Roth, S. The Structure of Suspended Graphene Sheets. *Nature* **2007**, *446*, 60–63.
20. Bao, W.; Miao, F.; Chen, Z.; Zang, H.; Jang, W.; Dames, C.; Lau, C. N. Controlled Ripple Texturing of Suspended Graphene and Ultrathin Graphite Membranes. *Nat. Nanotechnol.* **2009**, *4*, 562–566.
21. Nelson, D.; Piran, D. R.; Weinberg, S. *Statistical Mechanics of Membranes and Surfaces*; World Scientific: Singapore, 2004.
22. Radzikowski, L.; Le Doussal, P. Self-Consistent Theory of Polymerized Membranes. *Phys. Rev. Lett.* **1992**, *69*, 1209–1212.
23. Carlsson, J. M. Graphene: Buckle or Break. *Nat. Mater.* **2007**, *6*, 801–802.
24. Peierls, R. E. Bemerkungen uber Umwaldlungstemperaturen. *Helv. Phys. Acta* **1934**, *7*, 81–83.
25. Landau, L. D. Zur Theorie der Phasenumwandlungen II. *Phys. Z. Sowietunion* **1937**, *11*, 26–35.
26. Mermin, N. D. Crystalline Order in Two Dimensions. *Phys. Rev.* **1968**, *176*, 250–254.
27. Fasolino, A.; Los, J. H.; Katsnelson, M. I. Intrinsic Ripples in Graphene. *Nat. Mater.* **2008**, *6*, 858–861.
28. Zakharchenko, K. V.; Katsnelson, M. I.; Fasolino, A. Finite Temperature Lattice Properties of Graphene beyond the Quasiharmonic Approximation. *Phys. Rev. Lett.* **2009**, *102*, 046808.
29. Stolyarova, E.; Rim, K. T.; Ryu, S.; Maultzsch, J.; Kim, P.; Brus, L. E.; Heinz, T. F.; Hybertsen, M. S.; Flynn, G. W. High-Resolution Scanning Tunneling Microscopy Imaging of Mesoscopic Graphene Sheets on an Insulating Surface. *Proc. Natl. Acad. Sci. U.S.A.* **2007**, *104*, 9209–9212.
30. Tikhonenko, F. V.; Horsell, D. W.; Gorbachev, R. V.; Savchenko, A. K. Weak Localization in Graphene Flakes. *Phys. Rev. Lett.* **2008**, *100*, 056802.
31. Geringer, V.; Liebmann, M.; Echtermeyer, T.; Runte, S.; Schmidt, M.; Rückamp, R.; Lemme, M. C.; Morgenstern, M. Intrinsic and Extrinsic Corrugation of Monolayer Graphene Deposited on SiO_2. *Phys. Rev. Lett.* **2009**, *102*, 076102.
32. Bauer, E. Low Energy Electron Microscopy. *Rep. Prog. Phys.* **1994**, *57*, 895–938.
33. Bauer, E. *LEEM and SPLEEM in Science of Microscopy*; Hawkes, P. W., Spence, J. C., Eds.; Springer: Berlin, 2007; Vol. 1, pp 605−655.
34. Altman, M. S.; Chung, W. F.; He, Z. Q.; Poon, H. C.; Tong, S. Y. Quantum Size Effect in Low Energy Electron Diffraction of Thin Films. *App. Surf. Sci.* **2001**, *169*, 82–87.
35. Man, K. L.; Qiu, Z. Q.; Altman, M. S. Kinetic Limitations in Electronic Growth of Ag Films on Fe(100). *Phys. Rev. Lett.* **2004**, *93*, 236104.
36. Paggel, J. J.; Miller, T.; Chiang, T.-C. Occupied and Unoccupied Band Structure of Ag(100) Determined by Photoemission from Ag Quantum Wells and Bulk Samples. *Phys. Rev. B* **2000**, *61*, 1804–1810.
37. Wu, Y. Z.; Schmid, A. K.; Altman, M. S.; Jin, X. F.; Qiu, Z. Q. Spin-Dependent Fabry-Pérot Interference from a Cu Thin Film Grown on fcc Co(001). *Phys. Rev. Lett.* **2005**, *94*, 027201.
38. Altman, M. S. Low Energy Electron Microscopy of Quantum Well Resonances in Ag Films on W(110). *J. Phys.: Condens. Matter* **2005**, *17*, S1305–S1310.
39. Hibino, H.; Kageshima, H.; Maeda, F.; Nagase, M.; Kobayashi, Y.; Yamaguchi, H. Microscopic Thickness Determination of Thin Graphite Films Formed on SiC from Quantized Oscillation in Reflectivity of Low-Energy Electrons. *Phys. Rev. B* **2008**, *77*, 075413.
40. Ohta, T.; El Gabaly, F.; Bostwick, A.; McChesney, J. L.; Emtsev, K. V.; Schmid, A. K.; Seyller, T.; Horn, K.; Rotenberg, E. Morphology of Graphene Thin Film Growth on SiC(0001). *New J. Phys.* **2008**, *10*, 023034.
41. In the homogeneous field approximation, the acceptance angle of the LEEM microscope is given by $\alpha = \arcsin(r/f \cdot (E/E_0)^{1/2})$, where E_0 is the kinetic energy (start energy) of the electron, E the high voltage applied to the cathode lens (18 kV), f the focal length of objective lens (40 mm), and r the radius of the contrast aperture. At electron energy of 10 eV and contrast aperture of 30 μm, we estimate an acceptance half-cone of 1.8°.
42. Gass, M. H.; Bangert, U.; Bleloch, A. L.; Wang, P.; Nair, R. R.; Geim, A. K. Free-Standing Graphene at Atomic Resolution. *Nat. Nanotechnol.* **2008**, *3*, 676–681.
43. Yang, H.-N.; Wang, G.-C.; Lu, T.-M. *Diffraction from Rough Surfaces and Dynamic Growth Fronts*; World Scientific Publishing: Singapore, 1993.
44. Zhao, Y.; Wang, G.-C.; Lu, T.-M. Characterisation of Amorphous and Crystalline Rough Surface: Principles and Applications. In *Experimental Methods in the Physical Sciences*; Academic Press: New York, 2001; Vol. 37.
45. Lu, T.-M.; Lagally, M. G. Diffraction from Surfaces with Randomly Distributed Steps. *Surf. Sci.* **1982**, *120*, 47.
46. Yang, H.-N.; Lu, T.-M.; Wang, G.-C. Time-Invariant Structure Factor in an Epitaxial Growth Front. *Phys. Rev. Lett.* **1992**, *68*, 2612–2615.
47. Yang, H.-N.; Wang, G.-C.; Lu, T.-M. Instability in Low Temperature Molecular-Beam Epitaxy Growth of Si/Si(111). *Phys. Rev. Lett.* **1993**, *73*, 2348–2351.
48. Yang, H.-N.; Lu, T.-M.; Wang, G.-C. Diffraction from Diffusion Barrier Induced Mound Structures in Epitaxial Growth Fronts. *Phys. Rev. B* **1998**, *57*, 1922–1934.
49. Yang, H.-N.; Lu, T.-M.; Wang, G.-C. Diffraction from Surface Growth Front. *Phys. Rev. B* **1993**, *47*, 3911–3922.
50. For the range of electron energies used in our LEED experiments, $k_\perp \geq 5$ Å^{-1}; according to the literature, w varies in the range of a few angstroms to 1 nm. Therefore, the requirement $\Omega \gg 1$ is readily satisfied.
51. A comparison of η values for different thickness is possible in this case because $\alpha \sim 0.8$ for all multilayer samples.
52. Knox, K. R.; Wang, S.; Morgante, A.; Cvetko, D.; Locatelli, A.; Menteş, T. O.; Niño, M. Á.; Kim, P.; Osgood, R. M., Jr.

Spectromicroscopy of Single and Multilayer Graphene Supported by a Weakly Interacting Substrate. *Phys. Rev. B* **2008**, *78*, 201408(R).

53. Buseck, P. R.; Cowley, J. M.; Eyring, L. *High-Resolution Transmission Electron Microscopy*; Oxford University Press: Oxford, UK, 1988.
54. Locatelli, A.; Aballe, L.; Menteş, T. O.; Kiskinova, M.; Bauer, E. Photoemission Electron Microscopy with Chemical Sensitivity: SPELEEM Methods and Applications. *Surf. Interface Anal.* **2006**, *38*, 1554–1557.
55. Menteş, T. O.; Locatelli, A.; Aballe, L.; Pavlovska, A.; Bauer, E.; Pabisiak, T.; Kiejna, A. Surface Modification of Oxides by Electron-Stimulated Desorption for Growth-Mode Control of Metal Films: Experiment and Density-Functional Calculations. *Phys. Rev. B* **2007**, *76*, 155413.
56. Blake, P.; Novoselov, K. S.; Castro Neto, A. H.; Jiang, D.; Yang, R.; Booth, T. J.; Geim, A. K.; Hill, E. W. Making Graphene Visible. *Appl. Phys. Lett.* **2007**, *91*, 063124.
57. Takahashi, T.; Tokailin, H.; Sagawa, T. Angle-Resolved Ultraviolet Photoelectron Spectroscopy of the Unoccupied Band Structure of Graphite. *Phys. Rev. B* **1985**, *32*, 8317–8324.